Subduction Thermal Regime, Slab Dehydration, and Seismicity Distribution Beneath Hikurangi Based on 3-D Simulations

Suenaga, Nobuaki
Ji, Yingfeng
Yoshioka, Shoichi
Feng, Deshan

(Citation)
Journal of Geophysical Research: Solid,123(4):3080-3097

(Issue Date)
2018-04

(Resource Type)
journal article

(Version)
Version of Record

(URL)
https://hdl.handle.net/20.500.14094/90005030

Journal of Geophysical Research: Solid Earth

RESEARCH ARTICLE
10.1002/2017JB015382

Key Points:
- A remarkable interface slab dehydration band along Kapiti-Manawatu-Raukumara (KMR) is identified beneath Hikurangi by 3-D thermal modeling
- Interface ordinary earthquakes, tectonic tremors, and deep SSEs beneath Hikurangi are found actively occurring along KMR
- Plate interface beneath Manawatsu where tectonic tremors occurred is associated with high intraslab temperature gradient and high slab dehydration

Correspondence to:
Y. Ji and D. Feng,
jiyf@people.kobe-u.ac.jp;
fengdeshan@126.com

Citation:
Suenaga, N., Ji, Y., Yoshioka, S., & Feng, D. (2018). Subduction thermal regime, slab dehydration, and seismicity distribution beneath Hikurangi based on 3-D simulations. *Journal of Geophysical Research: Solid Earth*, *123*, 3080–3097. https://doi.org/10.1002/2017JB015382

Received 22 DEC 2017
Accepted 11 MAR 2018
Accepted article online 25 MAR 2018
Published online 22 APR 2018

Subduction Thermal Regime, Slab Dehydration, and Seismicity Distribution Beneath Hikurangi Based on 3-D Simulations

Nobuaki Suenaga[1], Yingfeng Ji[1], Shoichi Yoshioka[1,2], and Deshan Feng[3]

[1]Research Center for Urban Safety and Security, Kobe University, Kobe, Japan, [2]Department of Planetology, Graduate School of Science, Kobe University, Kobe, Japan, [3]School of Geoscience and Info-physics, Central South University, Changsha, China

Abstract The downdip limit of seismogenic interfaces inferred from the subduction thermal regime by thermal models has been suggested to relate to the faulting instability caused by the brittle failure regime in various plate convergent systems. However, the featured three-dimensional thermal state, especially along the horizontal (trench-parallel) direction of a subducted oceanic plate, remains poorly constrained. To robustly investigate and further map the horizontal (trench-parallel) distribution of the subduction regime and subsequently induced slab dewatering in a descending plate beneath a convergent margin, we construct a regional thermal model that incorporates an up-to-date three-dimensional slab geometry and the MORVEL plate velocity to simulate the plate subduction history in Hikurangi. Our calculations suggest an identified thrust zone featuring remarkable slab dehydration near the Taupo volcanic arc in the North Island distributed in the Kapiti, Manawatu, and Raukumara region. The calculated average subduction-associated slab dehydration of 0.09 to 0.12 wt%/km is greater than the dehydration in other portions of the descending slab and possibly contributes to an along-arc variation in the interplate pore fluid pressure. A large-scale slab dehydration (>0.05 wt%/km) and a high thermal gradient (>4 °C/km) are also identified in the Kapiti, Manawatu, and Raukumara region and are associated with frequent deep slow slip events. An intraslab dehydration that exceeds 0.2 wt%/km beneath Manawatu near the source region of tectonic tremors suggests an unknown relationship in the genesis of slow earthquakes.

1. Introductions

Large earthquakes have struck the Hikurangi margin offshore the eastern North Island of New Zealand, such as the 1931 M7.8 earthquake at Hawke's Bay, where six subsidence events have occurred over the past 7,000 years based on micropaleontological evidence (Cochran et al., 2006; Hayward et al., 2006). Along the Hikurangi trough, the Cretaceous Hikurangi Plateau that subducts beneath the Australian plate (Figure 1a) is thought to combine rupture of the interface and adjacent crustal faulting (e.g., Bai et al., 2017; Cochran et al., 2006). The national seismic hazard model for New Zealand uses geological models and seismological data to suggest that large to great earthquakes could occur on the subduction interface on the order of every 600–2,000 years (Stirling et al., 2002, 2012). In addition, the occurrence of the 2016 Kaikoura earthquake (Mw7.8) at the southern end of the Hikurangi margin indicates that the megathrust may be more seismically active than previously thought. Evidence shows that the coseismic slip of the Kaikoura earthquake probably also involved intracrustal faults as the main participants during the earthquake, resulting in the different seismic hazards on the ground (Furlong & Herman, 2017). The events continuously recorded by the dense local seismic network of the New Zealand Geonet Project (Geonet) spanning more than 10 years suggest a subduction interface beneath the North Island that is characterized by frequent small and medium interplate earthquakes extending to depth (Figure 1b).

The recent decades have witnessed discoveries of slow earthquakes recognized as a new category of slip behavior in various subduction zones (e.g., Audet et al., 2009; Dragert et al., 2001; Obara, 2002; Rogers & Dragert, 2003; Wech & Creager, 2011). In the eastern Alaska subduction zone, the connection between plateau subduction and tectonic tremors has recently been examined (e.g., Wech, 2016). Geodetic observations show strong potential (e.g., Wallace et al., 2004, 2009) in estimating interseismic slip deficits and the location of the slow slip events (SSEs) occurring in North Island, including the Hawke's Bay, Mahia Peninsula, and Poverty Bay region in central-northern Hikurangi and the Kapiti-Manawatu-Kaimanawa region in central-southern

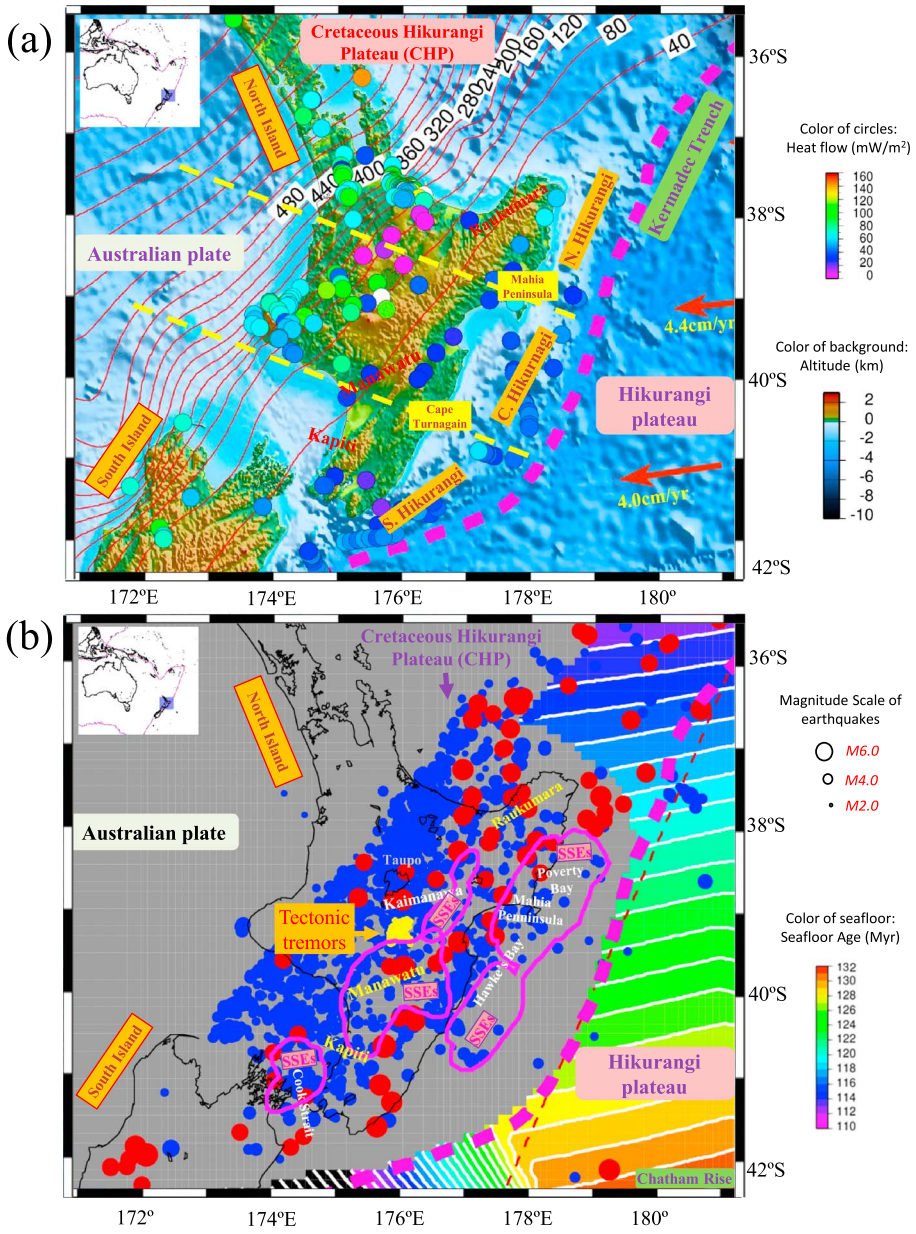

Figure 1. (a) Tectonic map of the Hikurangi subduction zone. The thick pink dashed line represents the plate boundary. The red lines indicate extrapolations of the isodepth contours (Williams et al., 2013) on the upper surface of the Cretaceous Hikurangi Plateau. The contour interval is 40 km. The red arrows indicate the plate convergence rate and the direction of the Hikurangi Plateau motion with respect to the Australian plate. The colored circles present the land-based surface heat flow observations from the global heat flow database (Pollack et al., 1993) and marine bottom-simulating reflector data (Townend, 1997). (b) Seafloor age of the Hikurangi Plateau (Müller et al., 2008). The solid red circles indicate the epicenters of earthquakes during a period from 1 January 1900 to 31 December 2000 from the Centennial Database. The solid blue circles represent the epicenters of earthquakes from 1 January 2001 to 31 December 2015 from Geonet. The thin dashed red line indicates the seaward model boundary. The patches encircled by pink lines correspond to horizontal projections of the source areas of SSEs (Wallace & Eberhart-Phillips, 2013), and the clustered small yellow circles at Manawatu indicate the epicenters of tectonic tremors from 1 August 2004 to 30 April 2012 (Idehara et al., 2014).

Hikurangi (Figure 1b; here Manawatu refers to the Manawatu-Wanganui region). Tectonic tremors have been filtered and identified at the downdip of a strongly coupled interface beneath Manawatu (e.g., Liu et al., 2010). The located tectonic tremors, SSEs, and coupled megathrusts vary from deeper in the south to shallower in northern Hikurangi (Wallace et al., 2009; Wallace & Eberhart-Phillips, 2013), which may imply an along-arc variability of the interplate thermal structure (e.g., Yabe et al., 2014).

To further interpret the coupling strength and thermally controlled downdip extent of the brittle failure affecting the faulting behaviors in Hikurangi, a featured subduction thermal regime was studied in previous thermal models, which obtained numerous constructive results. Wada and Wang (2009) successfully estimated a two-dimensional (2-D) thermal regime for the subduction thrust at Hikurangi using the PGCtherm model along a trench-normal profile. Yabe et al. (2014) interpreted the along-arc variability of the thermal structure in Hikurangi in terms of variability in the plate convergence rate and interplate friction. McCaffrey et al. (2008), using a 2-D thermal model, proposed that both the SSEs and the observed transition zone to the east of the North Island occurred at temperatures of 100 °C and suggested that temperature is not the sole dominant factor in either slow slip or fault-locking processes. Interplate temperature has been proposed to control the downdip extent of brittle failure, thereby influencing the distribution of interplate earthquakes; however, any effect in the third dimension (along-trench) has been poorly studied.

If the thermal models include an integrated three-dimensional (3-D) slab geometry for the thermal regime analysis and for estimating the associated 3-D slab dehydration inside the slab as well as a possible technical approximation of how the 3-D thermohydraulic state could affect the occurrence of subduction earthquakes in Hikurangi, the understanding of these issues may be greatly improved. For these reasons, we apply a thermomechanical kinematic model developed from the code Stag3D (Tackley & Xie, 2003) and 3-D analysis techniques (Ji et al., 2016, 2017; Ji & Yoshioka, 2017; Yoshioka & Murakami, 2007) to the Hikurangi subduction zone to investigate the subduction thermal regime and slab dehydration distribution from a 3-D (along-strike) perspective.

2. Methods and Models

2.1. Governing Equations

In our numerical models, the governing equations are constituted by the conservation of mass, momentum, and energy based on the anelastic liquid approximation (e.g., Ji et al., 2016; Yoshioka & Murakami, 2007):

$$\nabla\cdot(\rho\mathbf{v}) = 0, \tag{1}$$

$$-\nabla P + \nabla(\nabla\boldsymbol{\tau}) - \delta_{i3}\rho g\alpha\Delta T = 0, \text{ and} \tag{2}$$

$$\rho C_p\left(\frac{\partial T}{\partial t} + \mathbf{v}\cdot\nabla T\right) = k\nabla^2 T + \boldsymbol{\tau}\dot{\boldsymbol{\varepsilon}} + \delta_{i3}\rho g\alpha T v_3 + \rho H_r \tag{3}$$

In equation (1), ρ indicates the density and $\mathbf{v}$ is the flow velocity vector. In equation (2), P represents the pressure deviation from hydrostatic pressure, $\boldsymbol{\tau}$ means the deviatoric stress tensor, δ_{ij} indicates the Kronecker delta, g is the gravitational acceleration, α represents the reference thermal expansivity, and ΔT means the temperature difference relative to the surface. In equation (3), C_p indicates the specific heat at a constant pressure, T is the temperature, k represents the thermal conductivity, $\dot{\varepsilon}$ means the strain rate tensor, v_3 indicates the flow velocity component in the vertical direction, and H_r is the internal radioactive heating per unit mass. Equation (3) consists of an advection term, $\rho C_p\mathbf{v}\cdot\nabla T$; a thermal diffusion term, $k\nabla^2 T$; a viscous dissipation term, $\boldsymbol{\tau}\dot{\boldsymbol{\varepsilon}}$; an adiabatic heating term, $\delta_{i3}\rho g\alpha T v_3$; and a radioactive heating term, ρH_r.

2.2. Model Setup

We define the subduction velocity components by defining the subduction velocity in the subducted oceanic plate, which is dependent on the slab topography. The up-to-date plate geometry of the Hikurangi Plateau (Williams et al., 2013) is incorporated, using new seismicity and seismic reflection data with broader coverage than that in the model presented by Ansell and Bannister (1996). The subduction velocity follows the slab slope in the subduction direction, assuming that the slab geometry is fixed. Therefore, the velocity components along the x, y, and z directions (Figure 2a) are obtained (e.g., Ji et al., 2016):

$$v_x(x,y,z) = \frac{-2a(x,y)b(x,y)v_y + \sqrt{\left\{2a(x,y)b(x,y)v_y\right\}^2 - 4\left\{a(x,y)^2+1\right\}\left[\left\{a(x,y)^2+1\right\}v_y^2 - v^2\right]}}{2\left\{a(x,y)^2+1\right\}}, \tag{4}$$

$$v_y(x,y,z) = v_y, \text{ and} \tag{5}$$

$$v_z(x,y,z) = a(x,y)v_x + b(x,y)v_y, \tag{6}$$

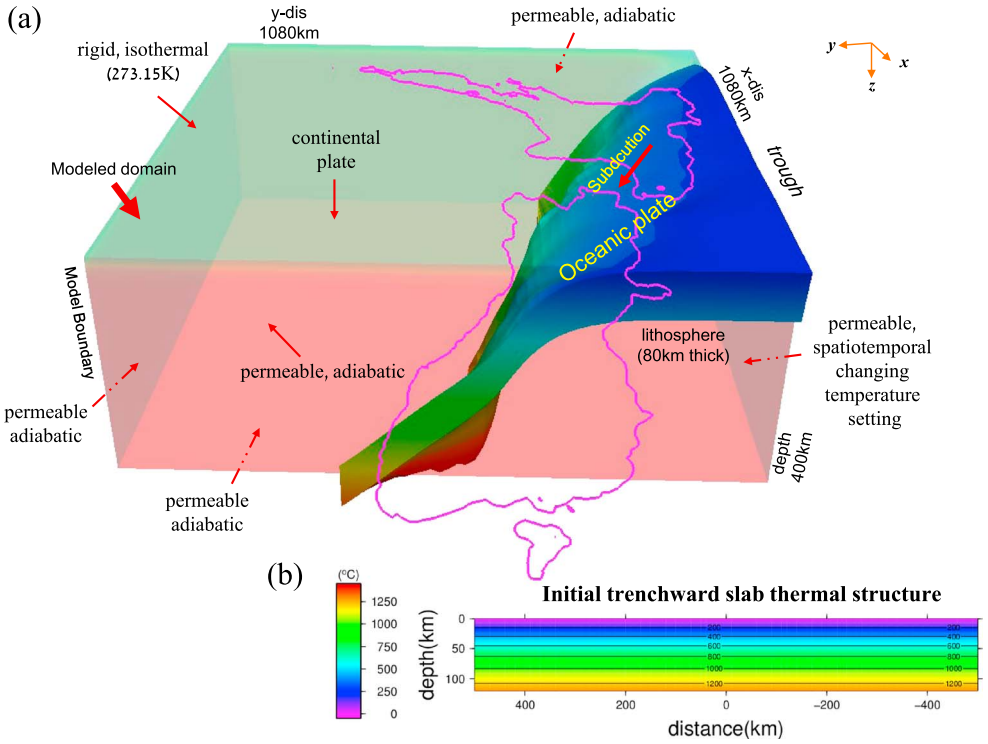

Figure 2. (a) Model setup including the model domain, dimensions, and boundary conditions. Warmer colors of the slab indicate deeper depths. (b) Initial slab temperature (24 Ma) ascribed to the subducting Hikurangi Plateau along the Hikurangi trench.

with

$$a(x,y) = \frac{1}{2}\{Z(x+\Delta x,y) - Z(x-\Delta x,y)\}\cdot\frac{z_{\max}}{x_{\max}}, \quad \text{and} \tag{7}$$

$$b(x,y) = \frac{1}{2}\{Z(x+\Delta x,y+\Delta y) - Z(x+\Delta x,y) + Z(x-\Delta x,y) - Z(x-\Delta x,y-\Delta y)\}\cdot\frac{z_{\max}}{y_{\max}}. \tag{8}$$

In equations (4)–(8), v indicates the subduction velocity obtained from interpolated MORVEL convergence rates (DeMets et al., 2010). The $v_x(x,y,z)$, $v_y(x,y,z)$, and $v_z(x,y,z)$ are the prescribed velocity components in the x, y, and z directions, respectively, in the subducting plate (Figure 2a). $Z(x,y)$ is the depth at the grid point (x,y). The Δx and Δy are the intervals of two neighboring grids along the x and y axes. In this study, the grid interval is $15 \times 15 \times 5$ km in the x, y, and z directions. The $x_{\max}$, $y_{\max}$, and $z_{\max}$ are the dimensions of the model. We prescribe the model size with $x_{\max}$ = 1,080 km in the trench-normal direction, $y_{\max}$ = 1,080 km in the trench-parallel direction, and $z_{\max}$ = 400 km in the vertical direction (Figure 2a).

For the trenchward temperature setting of the subducting plate, the time-dependent thermal structure is prescribed, following the plate cooling model to predict global seafloor heat flow (Grose & Afonso, 2013; McKenzie, 1967; Stein & Stein, 1992):

$$T(z,t_{oc}) = T_m\left[\frac{z}{d_0} + \frac{2}{\pi}\sum_{n=1}^{\infty}\frac{1}{n}\sin\left(\frac{n\pi z}{d_0}\right)\exp\left(\frac{-n^2\pi^2\kappa t_{oc}}{{d_0}^2}\right)\right]. \tag{9}$$

In equation (9), $T(z,t_{oc})$ indicates the temperature of the oceanic plate at a depth z and age t_{oc} along the Hikurangi Trench, T_m represents a lithospheric basal temperature, d_0 is the depth below which adiabatic heating is applied, and κ means the thermal diffusivity. The trenchward slab temperature is calculated at each time step. The age of the lithosphere has been estimated as approximately 130 Myr at the Hikurangi Plateau (Müller et al., 2008; Figure 1b). The trenchward thermal structure of the Cretaceous Hikurangi Plateau is assumed, following Yoshii (1975) (Figure 2b).

The rheological and thermal imposition of model boundaries involves permeable and adiabatic sidewalls and bottom and a rigid top at 0°C (Figure 2a). Frictional heating in the model follows Byerlee (1978) and Wang et al. (1995):

$$\tau_s = 0.85\sigma_n(1-\lambda) \quad [\sigma_n(1-\lambda) \le 200\text{MPa}], \text{and} \tag{10}$$

$$\tau_s = 50 + 0.6\sigma_n(1-\lambda) \quad [\sigma_n(1-\lambda) \ge 200\text{MPa}], \tag{11}$$

where τ_s indicates shear stress and σ_n represents the normal stress. The pore pressure ratio is

$$\lambda = \frac{P_f - P_d}{P_l - P_d}, \tag{12}$$

where P_f is the pore fluid pressure, P_d is the pressure at the Earth's surface, and P_l is the lithostatic pressure (Wang et al., 1995). Estimates of the pore fluid pressure along the Hikurangi margin have been inferred from observed *P* wave velocities (Bassett et al., 2014) and wedge taper analyses (Ellis et al., 2015; Fagereng & Ellis, 2009). Montserrat et al. (2012) suggested that high-porosity compressibility can maintain excess pore fluid pressure ratios. Yabe et al. (2014) calculated the interplate temperatures along three across-arc profiles in northern, central, and southern Hikurangi and proposed interplate coupling along with pore fluid pressure variations to interpret regional seismicity and slip behaviors, which is also used in this study. For the viscous flow law for wet olivine in the upper mantle, laboratory experiments have determined that diffusion creep (*df*) and dislocation creep (*ds*) accommodate a portion of the total strain rate (Billen & Hirth, 2007; Burkett & Billen, 2010; Hall & Parmentier, 2003; Hirth & Kohlstedt, 2003; Jadamec & Billen, 2010), which has also been included in the modeling with the equation

$$\dot{\varepsilon}_t = \dot{\varepsilon}_{df} + \dot{\varepsilon}_{ds}. \tag{13}$$

The composite upper mantle viscosity for deformation at a constant stress is

$$\eta_{comp} = \frac{\eta_{df}\eta_{ds}}{\eta_{df} + \eta_{ds}}, \tag{14}$$

where η_{df} and η_{ds} represent the diffusion creep and dislocation creep viscosities for olivine, respectively (Ranalli, 1995). The flow law constants for wet olivine aggregates for diffusion and dislocation creep from Table 1 in Hirth and Kohlstedt (2003) are used in this study.

The simulation period is set to 24 Myr from the initiation of plate subduction into the model domain to the present when the model domain including the subducted plate, the mantle wedge, and the continental plate reaches a steady thermal state.

2.3. Calculation Methods for Water Content and Slab Dehydration

The thermal results are subsequently utilized to estimate the water content in the subducted plate, using a phase diagram of hydrous mid-ocean ridge basalt (MORB) (Hacker, Abers, et al., 2003; Hacker, Peacock, et al., 2003; Omori et al., 2009) and ultramafic rocks (Hacker, Abers, et al., 2003; Hacker, Peacock, et al., 2003). In this way, we obtain the water content value at every grid point inside the subducting plate. Here the subducted plate is assumed to be fully saturated after such a long period of hydration, while some portions particularly in the upper mantle may remain undersaturated, and thus, the spatial heterogeneity in the state of slab hydration influences the pattern of dehydration and slab rehydration, but relative details remain poorly understood (e.g., Wada et al., 2012). Then, we compute the slab dehydration (variation in water content per unit length) at grids. First, we use interpolation to transform the water content values *wt* (*x*, *y*, *z*) (*x* and *y* are the horizontal distances, and *z* is the vertical distance of a node with a unit of km) into *wt* (*x*, *y*, *d*), which is under another coordinate system of (*x*, *y*, *d*) (*d* indicates the grid depth relative to the subduction interface with a unit of km). For example, *wt* (*x*, *y*, 0) represents the water content value at the node (*x*, *y*) on the subduction megathrust. Second, the water content differences between neighboring grids with the same depth from the interface (*d* value) along the subducting slab are computed as the slab dehydration at a grid (*x*, *y*, *d*)

$$\mathrm{dwt}(x,y,d) = \frac{\mathrm{wt}(x+1, y+\tan\alpha, d)\text{-}\mathrm{wt}(x\text{-}1, y\text{-}\tan\alpha, d)}{\sqrt{4 + 4\tan^2\alpha + \{z(x+1, y+\tan\alpha, d)\text{-}z(x\text{-}1, y\text{-}\tan\alpha, d)\}^2}}, \tag{15}$$

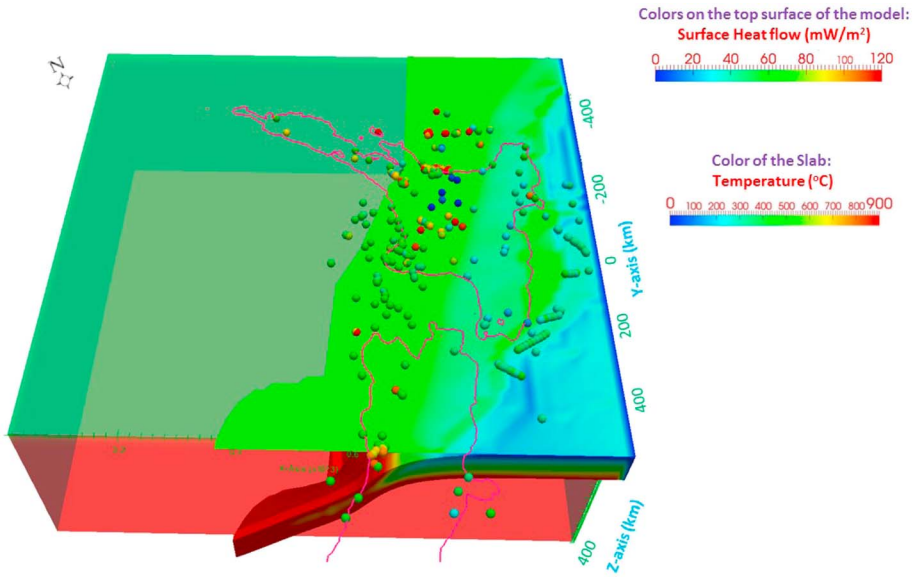

Figure 3. The observations (spheres) and calculations (colored top surface) of surface heat flow at Hikurangi. Observations include the global heat flow database (Pollack et al., 1993) and bottom-simulating reflector data (Townend, 1997). The transparent box is the model domain. The color of the subducted Hikurangi Plateau indicates the calculated slab temperature.

where α is the radius of subduction obliquity and z indicates the grid depth (km) from the Earth's surface. The final step is to transform the values of dwt (x, y, d) into dwt (x, y, z). Equation (15) can be used to calculate the temperature gradient if wt is replaced with temp (e.g., Ji & Yoshioka, 2017). The relationships with seismicity, tectonic tremors, and SSEs in Hikurangi are evaluated in a 3-D framework based on the calculation results.

2.4. Surface Heat Flow Observations Constraining the Model

To constrain the thermal model, the measurements of surface heat flow play an important role in the determining the model parameters for the numerical simulation. Our results fit the measurements well seaward, as shown in Figures 3–5. Heat flow observations include the data from our global heat flow database (Pollack et al., 1993) and the bottom-simulating reflectors (Henrys et al., 2003; Townend, 1997) (Figures 4 and 5). The abnormally high value of surface heat flow in the Taupo volcanic zone is attributable to the arc volcanism, which is not employed to constrain the thermal model.

3. Results

3.1. Calculated Slab Thermal Regime

Figure 6a presents the calculated thermal state of the upper surface of the Hikurangi Plateau. The isotherm contour of 200 °C projected on the Earth's surface is predicted to partly overlap with the eastern coast of the North Island. The 600–1,000 °C contours appear beneath the Taupo volcanic arc and are conjectured to contribute to arc volcanism. The Hikurangi Plateau subducts with a much greater dip angle beneath the back-arc basin than offshore eastern North Island. Thus, the downdip limit of the seismically ruptured interface is inferred to be located underneath the volcanic arc due to a mineral transition from brittle failure to creep deformation. The updip limit of such ruptures and shallow slips is poorly constrained by the seismic moment release (Furlong & Herman, 2017).

To compare our calculation of the slab thermal state, we employ the hypocenter data taken from Geonet for earthquakes with magnitudes >2.0 from 1 January 2001 to 31 December 2015 and from the Centennial Earthquake Database (Engdahl & Villasenor, 2002) for earthquakes with magnitudes >5.5 from 1 January 1900 to 31 December 2000. We follow the depth estimates proposed by the Centennial Earthquake Database; therefore, all historical >M7.0 earthquakes, including subduction-type events and others near the subduction interface, are involved in Figures 6 and 7. From the featured occurrence of interplate

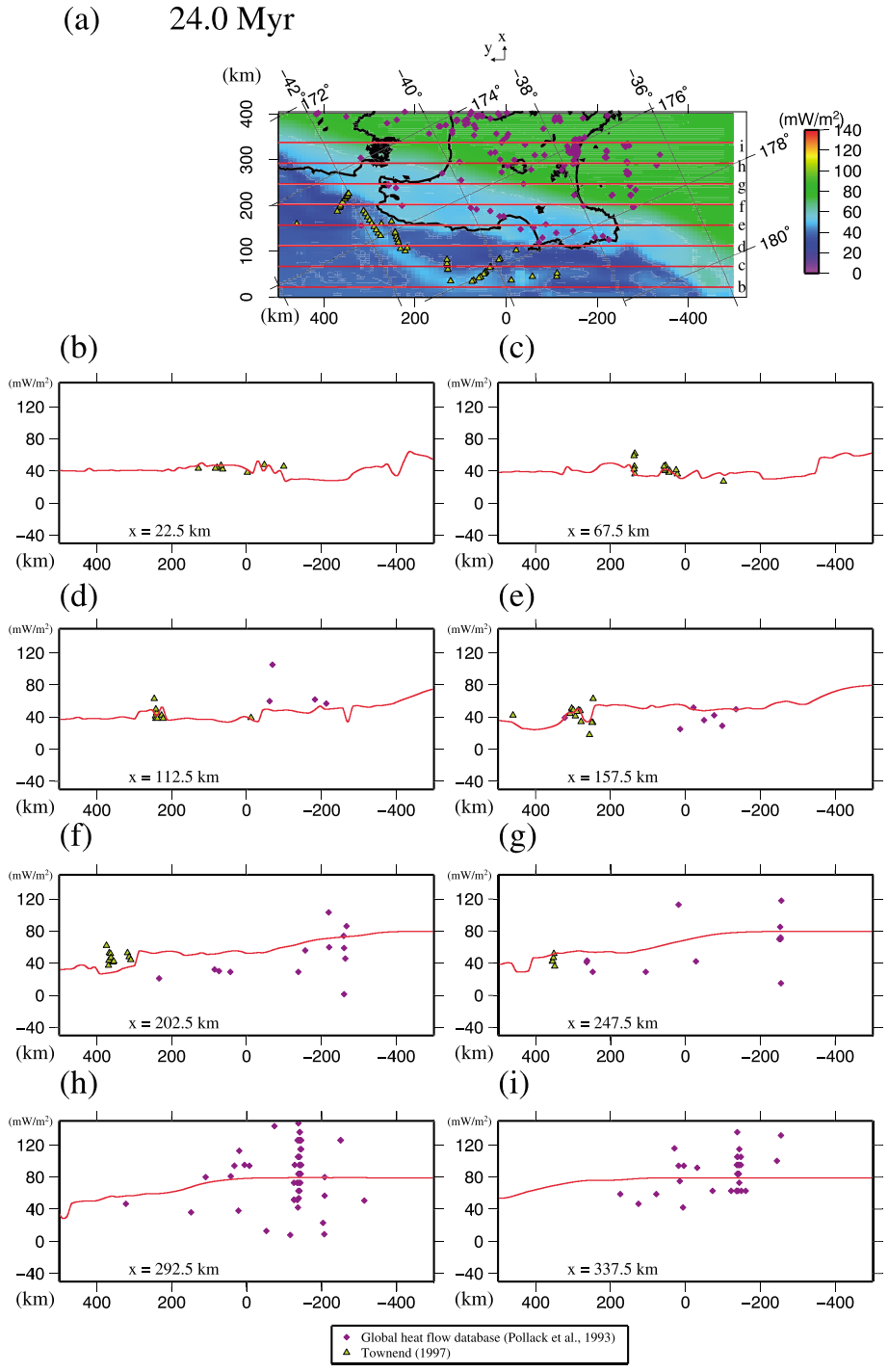

Figure 4. (a) Spatial distribution of the calculated surface heat flow of the thermal model at 24 Myr. The observations and calculations of surface heat flow are compared along the trench-parallel profiles b to i in (b) to (i), respectively. (b) The observations and calculations of surface heat flow along profile b (x = 22.5 km). The purple diamonds and yellow triangles denote heat flow data from the global heat flow database (Pollack et al., 1993) and the bottom-simulating reflectors (Townend, 1997), respectively, within a distance of 22.5 km from the profile. The red curve is the calculated heat flow. (c) Along profile c (x = 67.5 km). (d) Along profile d (x = 112.5 km). (e) Along profile e (x = 157.5 km). (f) Along profile f (x = 202.5 km). (g) Along profile g (x = 247.5 km). (h) Along profile h (x = 292.5 km). (i) Along profile i (x = 337.5 km).

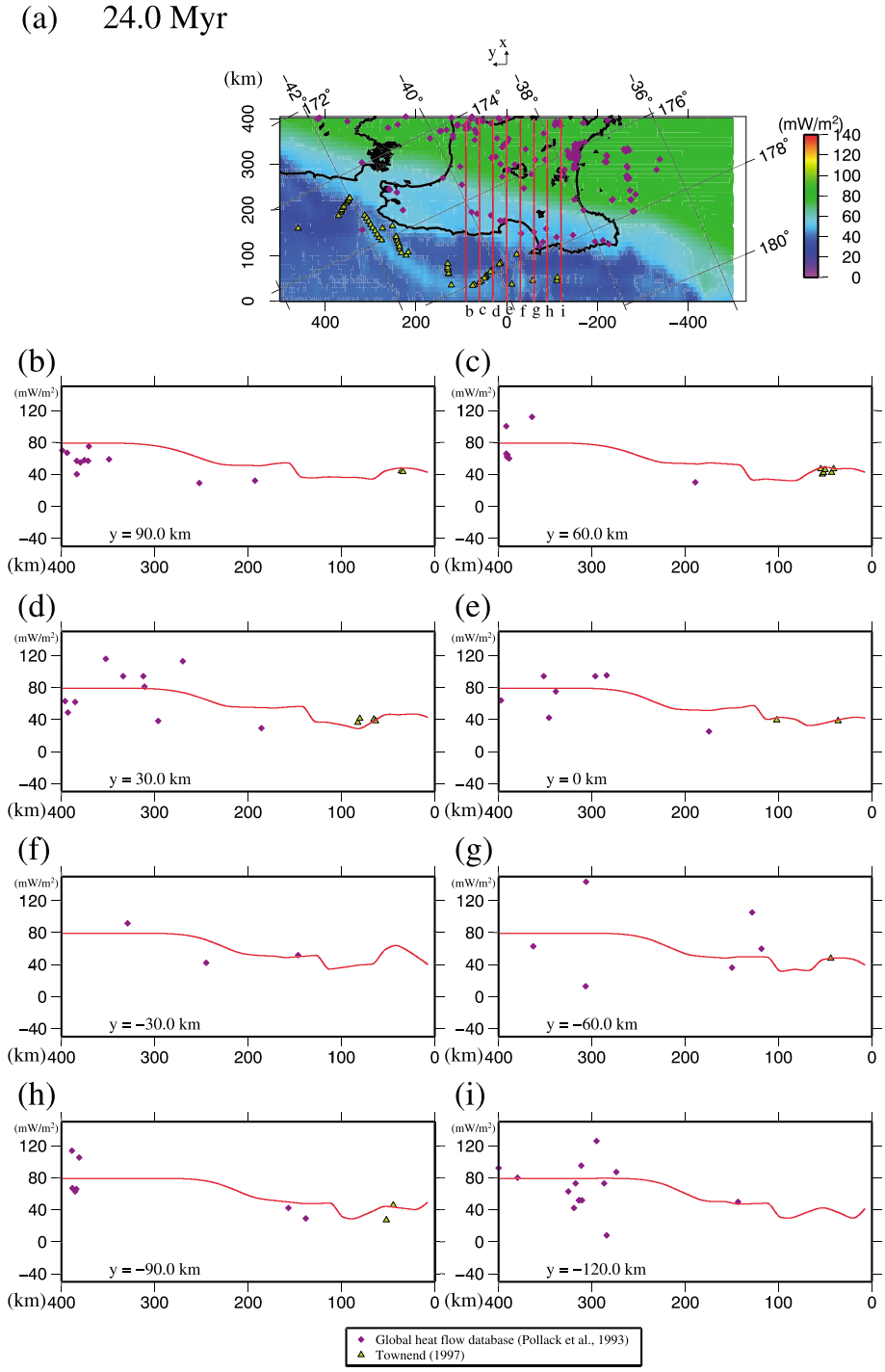

Figure 5. (a) Spatial distribution of the calculated surface heat flow of the thermal model at 24 Myr. The observations and calculations of surface heat flow are compared along the trench-normal profiles b to i in (b) to (i), respectively. (b) The observations and calculations of surface heat flow along profile b (y = 90.0 km). The purple diamonds and yellow triangles denote heat flow data from the global heat flow database (Pollack et al., 1993) and the bottom-simulating reflectors (Townend, 1997), respectively, within a distance of 15 km from the profile. The red curve is the calculated heat flow. (c) Along profile c (y = 60 km). (d) Along profile d (y = 30 km). (e) Along profile e (y = 0 km). (f) Along profile f (y = −30 km). (g) Along profile g (y = −60 km). (h) Along profile h (y = −90 km). (i) Along profile i (y = −120 km).

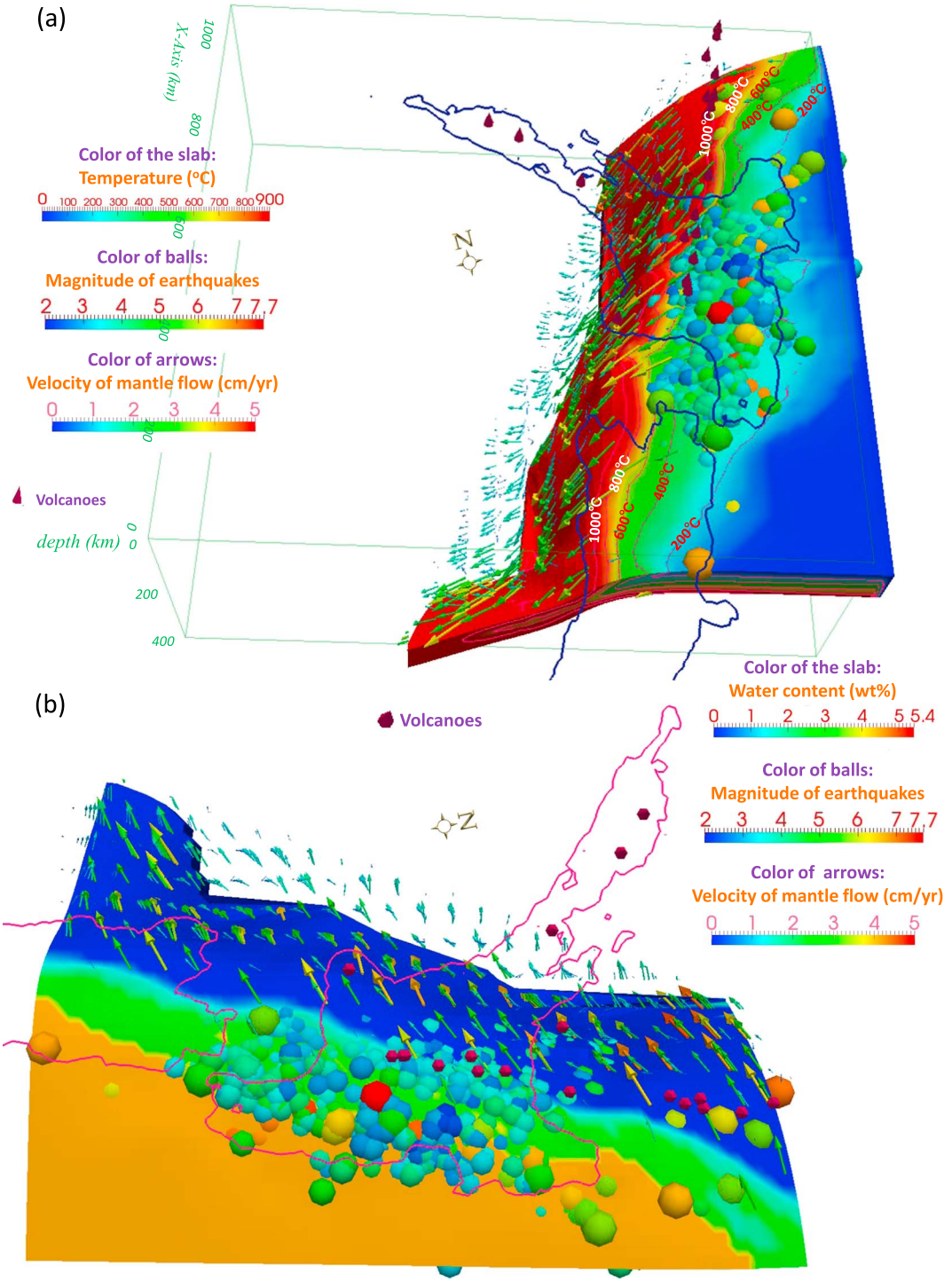

Figure 6. (a) 3-D view of the interplate temperature and induced flow velocity vectors in the mantle wedge beneath the Hikurangi subduction zone. The color of the slab surface indicates the temperature (°C). The red and white lines represent isothermal contour lines with an interval of 200 °C. The colored arrows represent the mantle flow induced by the subduction of the Hikurangi Plateau. The colored spheres indicate the hypocenters of interplate earthquakes of different magnitudes exceeding M5.5, which are also reflected by the radii of the spheres, from 1 January 1900 to 31 December 2000 (Centennial Database), and from 1 January 2001 to 31 December 2015 (Geonet). The red cones indicate volcanoes. The cuboid frame in green shows the modeled domain. (b) Same as (a) except that the plate color indicates the slab water content, viewed at a different point.

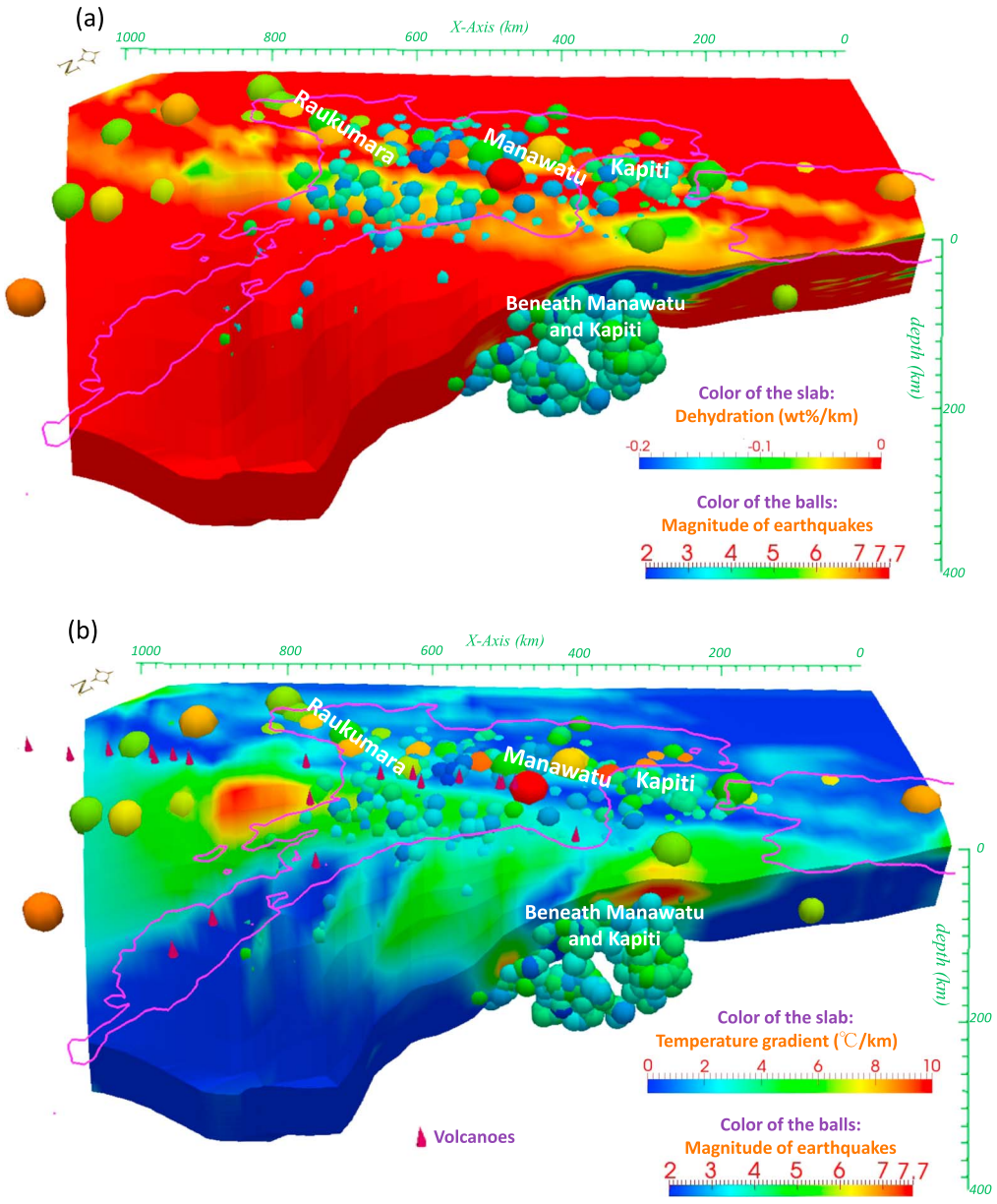

Figure 7. (a) 3-D view of the calculated slab dehydration (wt%/km) in the subducting direction along the slab geometry. The colored spheres indicate the hypocenters of earthquakes with magnitudes exceeding 5.5. The red cones are volcanoes. (b) Same as (a) except that the plate color indicates the calculated slab temperature gradient (°C/km) in the subducting direction along the slab geometry.

earthquakes for more than 10 years (Figure 6a), the 200 °C isothermal contour beneath the eastern coast indicates a potential updip limit for the regular earthquakes that often occur. The densely distributed inland earthquakes are prevailingly located between the volcanic arc and the eastern coast, approximately along the Kapiti, Manawatu, and Raukumara region (KMR; also shown in Figure 1). Adjacent to Cook Strait is a turning point for the subducting Hikurangi Plateau in the transition to the Alpine fault strike-slip regime beneath the South Island, and therefore, the inferred slab geometry beneath the South Island is uncertain due to a possible extrapolation of tomographic data (Furlong & Herman, 2017). Thus, we focus on the slab thermal regime beneath the North Island, mainly to the east of the Taupo volcanic arc, that is, the KMR region. Among them, most of the interplate >M5.5 earthquakes occurred at temperatures between 150 and 400 °C (Figure 6a), which correspond to brittle failure in the seismogenic zone (Hyndman & Wang, 1993; Hyndman, Wang, & Yamano, 1995).

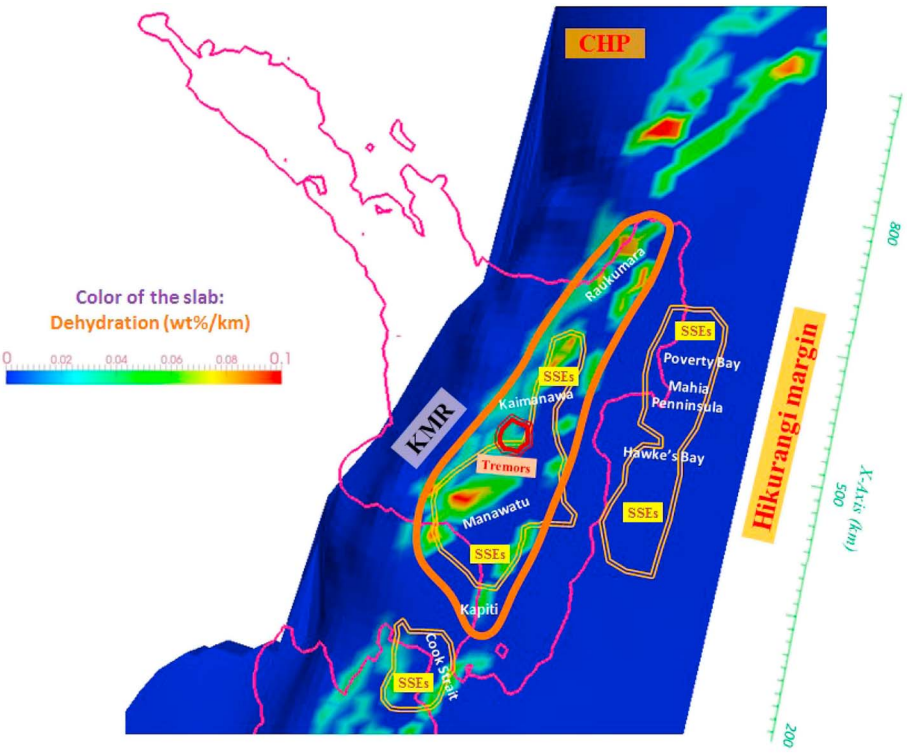

Figure 8. Horizontal projection of the spatial distribution of the calculated slab dehydration (wt%/km) on the plate interface. The source areas of the SSEs are encircled by double thin yellow lines, and the tectonic tremors are encircled by double red lines. The KMR region is encircled by a thick orange line.

3.2. Calculated Water Content

The water content distribution on the upper surface of the subducted plate beneath Hikurangi (Figure 6b) is further elucidated according to the phase diagrams of hydrous MORB (Omori et al., 2009) and ultramafic rocks (Hacker, Abers, et al., 2003; Hacker, Peacock, et al., 2003). In Figure 6b, we identify a remarkable dehydration band (the region from yellow to green and from green to blue) along the interplate seismogenic zone, in which most of the hypocenters of $>$M3 historical earthquakes are densely distributed along the KMR band sustainably through time in the model as a stable state. The water content of the hydrous minerals in the slab at the plate interface decreases from approximately 4.4 to 0.0 wt% with various dip angles across the KMR region (Figure 6b). The metamorphic process for MORB from the greenschist to the lawsonite blueschist facies is associated with a rapid temperature increase and water content decrease accompanied by an increasing 3-D slab dip angle in our result.

3.3. Slab Dehydration Distributions

Based on equation (15), we obtain the slab dehydration per unit length (wt%/km) of the whole subducting plate. Figure 7a shows the dehydration in units of wt%/km on the slab's upper surface and on a vertical cross section approximately 330 km from the Hikurangi margin. The slab dehydration exceeds 0.05 wt%/km along the KMR region. The deeper and thicker zone is geographically consistent with the SSEs in the Kapiti-Manawatu-Kaimanawa ranges (Figure 1b; e.g., Wallace & Eberhart-Phillips, 2013), which include the KMR seismic zone. We thus infer that the released and upwelling fluid from the deeper, thick dehydration zone strongly affects the KMR seismic zone (Figure 8). However, the shallower SSE source zones along Hawke's Bay, the Mahia Peninsula, and Poverty Bay (Wallace et al., 2009) are not associated with any apparent slab dehydration.

The temperature gradient on the upper surface in the subduction direction and the vertical cross section in Figure 7b indicates a thermal gradient exceeding 4 °C/km in the KMR region. This gradient is caused by the greater slab dip angle formed as a result of the significant slab curvature associated with oblique subduction at depth, which has also been observed at other subduction zones, such as western Shikoku and the Kii Peninsula in southwest Japan (Ji et al., 2016). A high thermal gradient is expected to lead to a rapid phase

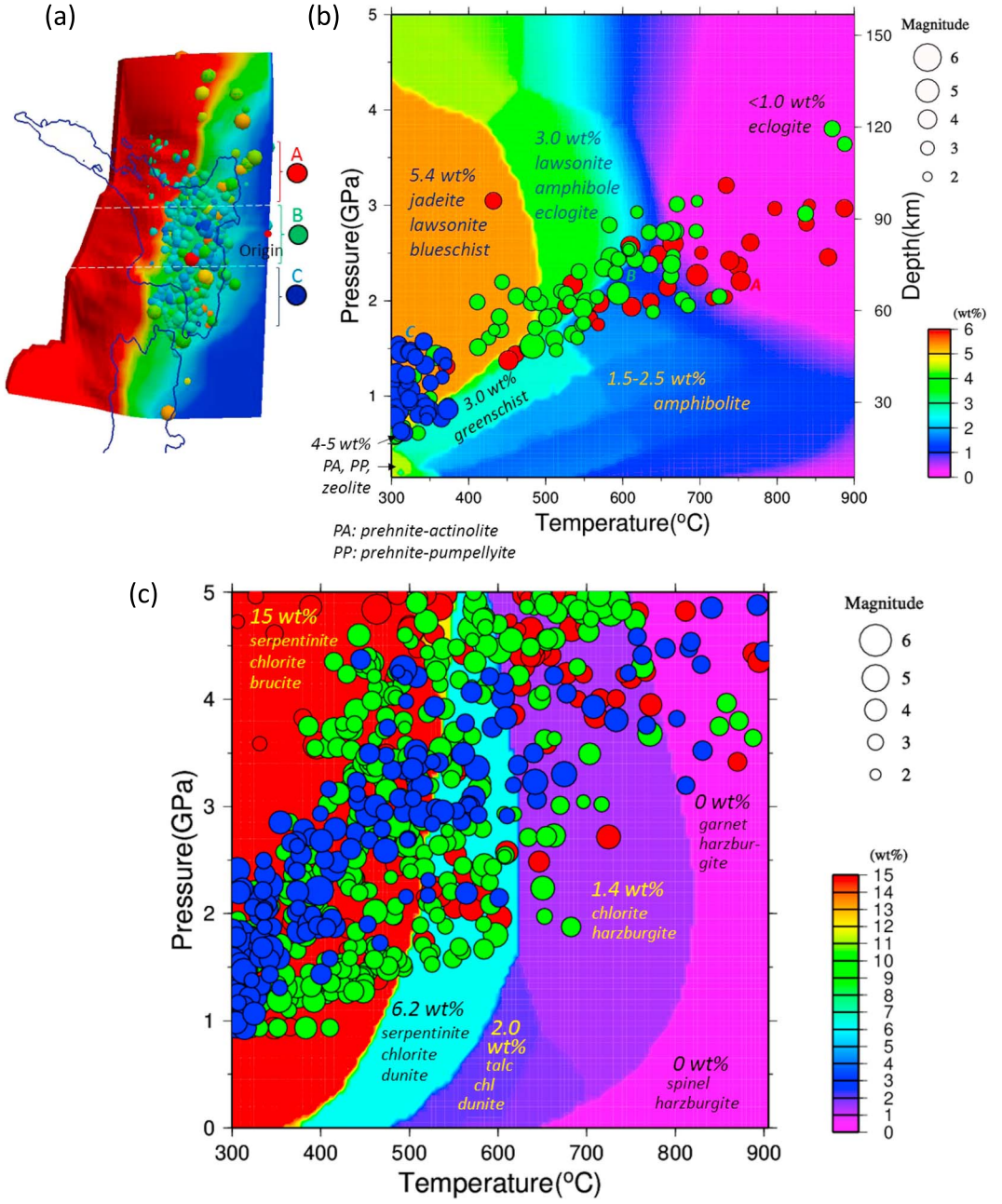

Figure 9. (a) Locations of zones A, B, and C with M > 2.0 earthquakes (spheres) obtained from Geonet (1 January 2001 to 31 December 2015) with depths <400 km. The three zones A, B, and C are separated by two white dashed lines. (b) The P-T condition of intraslab earthquakes plotted on the phase diagram of hydrous MORB (7 km thick) for the Hikurangi Plateau. The red, green, and blue solid circles indicate the hypocenters of the earthquakes in the three zones A, B, and C marked in (a), respectively. (c) The P-T condition of intraslab earthquakes plotted on the phase diagram for the ultramafic rocks inside the Hikurangi Plateau beneath the MORB layer of the oceanic crust.

transformation process within the intraslab hydrous minerals and contribute to immediate slab dehydration. That is, the slope of the subduction path in the P-T diagram is smaller than that which has a lower temperature gradient. Hence, the P-T path is directed quickly from highly hydrous minerals (Figure 9; e.g., blueschist, greenschist in Figure 9b and serpentinite in Figure 9c) to dehydrated assemblages (e.g., eclogite in Figure 9b and harzburgite in Figure 9c). A shorter path length in the P-T diagram corresponding to the same amount of slab dehydration (wt%) results in an increase in the effective slab dehydration. Thus, the way in which the slab thermal gradient influences the calculated slab dehydration can be partly interpreted. Interestingly, a significantly

Table 1
Temperature Condition, Maximum Slab Dehydration, and Thermal Gradient for the Located Earthquakes, slow slip events (SSEs), and Tectonic Tremors at Hikurangi

Slip behavior	Temperature condition	Maximum slab dehydration	Thermal gradient	Geographic location
Interplate earthquake	150–700 °C	>0.09 wt%/km	>4 °C/km	Raukumara, N. Hikurangi
	200–650 °C	>0.1 wt%/km	>4 °C/km	Manawatu, C. Hikurangi
	250–650 °C	>0.12 wt%/km	>7 °C/km	Kapiti, S. Hikurangi
SSEs	200–350 °C	<0.05 wt%/km	<4 °C/km	Offshore, N. Island
	350–550 °C	>0.1–0.12 wt%/km	>4–7 °C/km	Inland, N. Island
	350–550 °C	>0.08 wt%/km	>4 °C/km	Cook Strait
Tectonic tremors	300–650 °C	>0.2 wt%/km	>4–10 °C/km	Manawatu, C. Hikurangi

high intraslab thermal gradient is identified beneath Manawatu and Kapiti. Therefore, large values of the dehydration and a high temperature gradient occur simultaneously at depths of 40–50 km, where both deep SSEs and tectonic tremors have been detected (Figures 1b and 7b; e.g., Idehara et al., 2014). The tectonic tremors detected by Yabe et al. (2014) are distributed in the region adjacent to the local SSEs.

We summarize the thermohydraulic conditions for the earthquakes, tectonic tremors, and SSEs in the Hikurangi subduction zone in Table 1. The tectonic tremors are associated with a slab dehydration of more than 0.2 wt%/km and a temperature gradient higher than 10 °C/km. The values of the interplate dehydration beneath northern, central, and southern Hikurangi are estimated at approximately 0.09, 0.10, and 0.12 wt%/km, respectively, which potentially accounts for the along-arc variation in the interplate pore fluid pressure ratio (Fagereng & Ellis, 2009; Yabe et al., 2014). The correspondence between the geographical distributions is shown in Figure 8.

4. Discussion

4.1. Variations in Thermal Estimates and Limits

Several estimates of the temperature at the plate interface have been determined by previous thermal models at the Hikurangi subduction zone. For example, the temperature at the plate interface at a depth of 50 km has been estimated using 2-D models, including the values of 350–400 °C (Fagereng & Ellis, 2009), 400–450°C (McCaffrey et al., 2008), and 600°C (Yabe et al., 2014). In this study, the updated 3-D slab geometry and along-arc variation in the subduction velocity account for the differences from the previous estimates. The obtained interplate temperatures at a depth of 50 km are almost 500°C beneath northern Hikurangi, 450–500°C beneath central Hikurangi, and 400–450°C beneath southern Hikurangi. These results are closer to those of McCaffrey et al. (2008), probably due to an approximate initial temperature setting for continental and oceanic plates. This study includes the 3-D effect of subduction of the Hikurangi Plateau, and the calculated interplate temperatures differ by nearly 100°C at a depth of 50 km between southern and northern Hikurangi, which indicates a moderate fluctuation. However, a spatial variability in volcanic magma and radioactive heat generation has not been included, and these parameters probably account for the misfits between the calculations and observations of surface heat flow in the central-western North Island.

The Hikurangi Plateau consists of lawsonite blueschist, whereas lawsonite-bearing rocks rarely exist in hot subduction zones (Okazaki & Hirth, 2016). Figure 7a depicts the slab dehydration band near the 50 km isodepth, which has several deviations caused by the slab geometry that result in temperatures ranging from 400 to 500°C (Figure 6a). The KMR region is located between the brittle failure and the decoupled zone of creep deformation or stable sliding near the downdip seismogenic limit (Wallace et al., 2009), and the observed >M2 earthquakes occur farther downdip of geodetically locked seismogenic zones (Figure 6).

4.2. Interplate Coupling Based on Geodetic Observations and Slab Dehydration

The lower water release and higher interplate frictional heating in northern Hikurangi appear to conflict with the geodetic observation that a lower degree of interplate coupling in northern Hikurangi may accompany shallower SSEs (Wallace et al., 2009). However, the turbidite fill thickens southward from 0–1 km to the northeast of the North Island to 3–6 km to the northeast of the South Island (Lewis et al., 1998). Additionally, the shallow SSEs in the north occur at a depth of nearly 10 km (Bassett et al., 2014; Ellis et al., 2015), which is much shallower than the continental Moho depth. Hence, sediment thickening may account for both the low

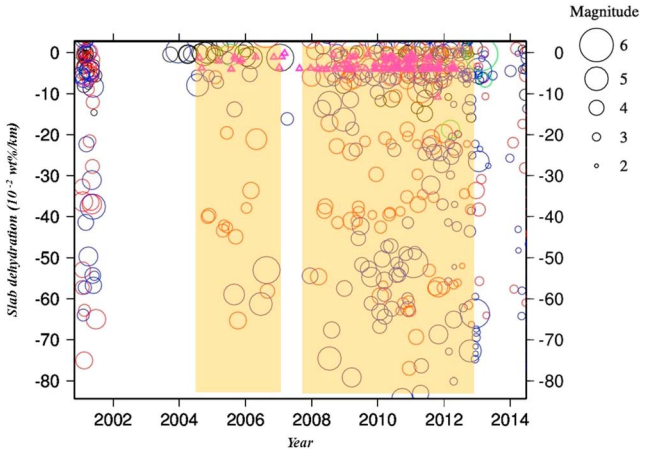

Figure 10. (a) The relationship between the slab dehydration and the year of earthquakes. The horizontal axis indicates the year of >M2 earthquakes recorded by Geonet from 1 January 2001 to 31 December 2015. The vertical axis indicates the slab dehydration at the hypocenters. The open circles indicate hypocenters with the colors showing the depth ranges vertically down from the upper surface of the subducted plate. Black: −2 to 7 km; red: 7 to 40 km; blue: 40 to 80 km; and green: > 80 km. The pink open triangles indicate the possible slab dehydration condition for the tectonic tremors. The transparent light orange columns indicate the synchronous activity between tectonic tremors and regular earthquakes beneath Manawatu.

surface heat flow in the north and the strong interplate coupling in the south because of the greater fault strength of a smooth plate interface than of a geometrically rough interface that slips by creeping (Gao & Wang, 2014). The along-arc variability in the subducted sediment layer is directly linked to the along-arc variation in the frictional properties. According to Wallace and Eberhart-Phillips (2013), the source region of the SSEs beneath the Hikurangi subduction zone comprises two parallel belt-like zones: an inland part below the Kapiti, Manawatu (Wallace et al., 2009), and Kaimanawa ranges (Wallace & Eberhart-Phillips, 2013) and the area located in the fore-arc offshore zone below Hawke's Bay, the Mahia Peninsula, and Poverty Bay (Wallace et al., 2009) in central-northern Hikurangi. Using a network of absolute pressure gauges on the seafloor, Wallace et al. (2016) found that the largest uplift displacement during the shallow SSE in September 2014 occurred near Poverty Bay offshore Gisborne. Furthermore, low-temperature (McCaffrey et al., 2008) and fluid-rich sediments (Bell et al., 2010) are present at depths of 4–7 km near the plate interface.

In addition, the dehydration of the sediment layer can supply adequate fluids to generate plate faulting and SSEs (Ellis et al., 2015). Clift and Vannucchi (2004) and van Keken et al. (2011) indicated that the along-arc variability in friction at the North Island might be caused by varying sediment thicknesses and sediment compaction rates offshore and that the total amount of released fluid may also be affected (e.g., Bassett et al., 2014; Saffer & Wallace, 2015; Wallace et al., 2009). We thus speculate that the subduction of the thermally heterogeneous plate produces an overpressured plate interface in the downdip portion that is interpreted as producing a slab metamorphic process associated with the deep SSEs, whereas in the shallow segment in the source region of the SSEs, the interplate stress could cause another type of dehydration, which is thought to be directly controlled by the fluid from sediment compaction and dehydration. The thermally controlled slab dehydration associated with phase transformations and the dehydration of subducted sediments are expected to be important factors in producing ample fluids for these SSE source regions.

4.3. Relationships Among Earthquakes, Tectonic Tremors, and Slab Dehydration

According to the Geonet earthquake catalog, regular earthquakes recorded at Manawatu occur at depths of 40 to 80 km, whereas tectonic tremors are only detected at depths of 10–50 km (Idehara et al., 2014). The slip areas of SSEs and adjacent slow earthquakes have also been reported in the Guerrero, Mexico, and Costa Rica subduction zones (Beroza & Ide, 2011; Yoshioka et al., 2004), which indicates an unknown connection within a broad range of slow and regular earthquakes. Most likely, the absolute strength of faults is influenced by the ambient fluid pressure, and the additional strength reduction in creeping zones may be due to transiently elevated fluid pressures (Hardebeck & Loveless, 2017) potentially derived from slab dehydration.

The subducting plate is divided into three along-arc zones A, B, and C (Figure 9a) to compare the occurrence of selected interplate earthquakes. The boundaries at distances of −70 and 110 km from the coordinate origin are represented by the two white dashed lines. Earthquakes with depths of 0–7 km below the plate interface are plotted on the MORB phase diagram (Omori et al., 2009; Figure 9b). Based on the estimated temperatures and the depth-related pressures, we inferred the P-T conditions in the three zones in the MORB, which are represented by different colors. The metamorphic process in southern Hikurangi (zone C in Figure 9a) corresponds to transitions from jadeite-lawsonite blueschist, prehnite-actinolite, prehnite-pumpellyite, or zeolite to greenschist (which indicates a lower dip angle). In contrast, central Hikurangi (zone B) favors a transition from jadeite-lawsonite blueschist to lawsonite-amphibole eclogite or amphibolite, and northern Hikurangi (zone A) favors a transition from greenschist to eclogite or amphibolite, which indicates a higher dip angle. The earthquakes in the MORB layer appeared to occur near the boundaries of phase transformations.

In addition, for the ultramafic rocks distributed >7 km beneath the upper surface of the slab, the phase transformations may also exhibit effects on intraslab earthquake patterns. One example is the transformation of

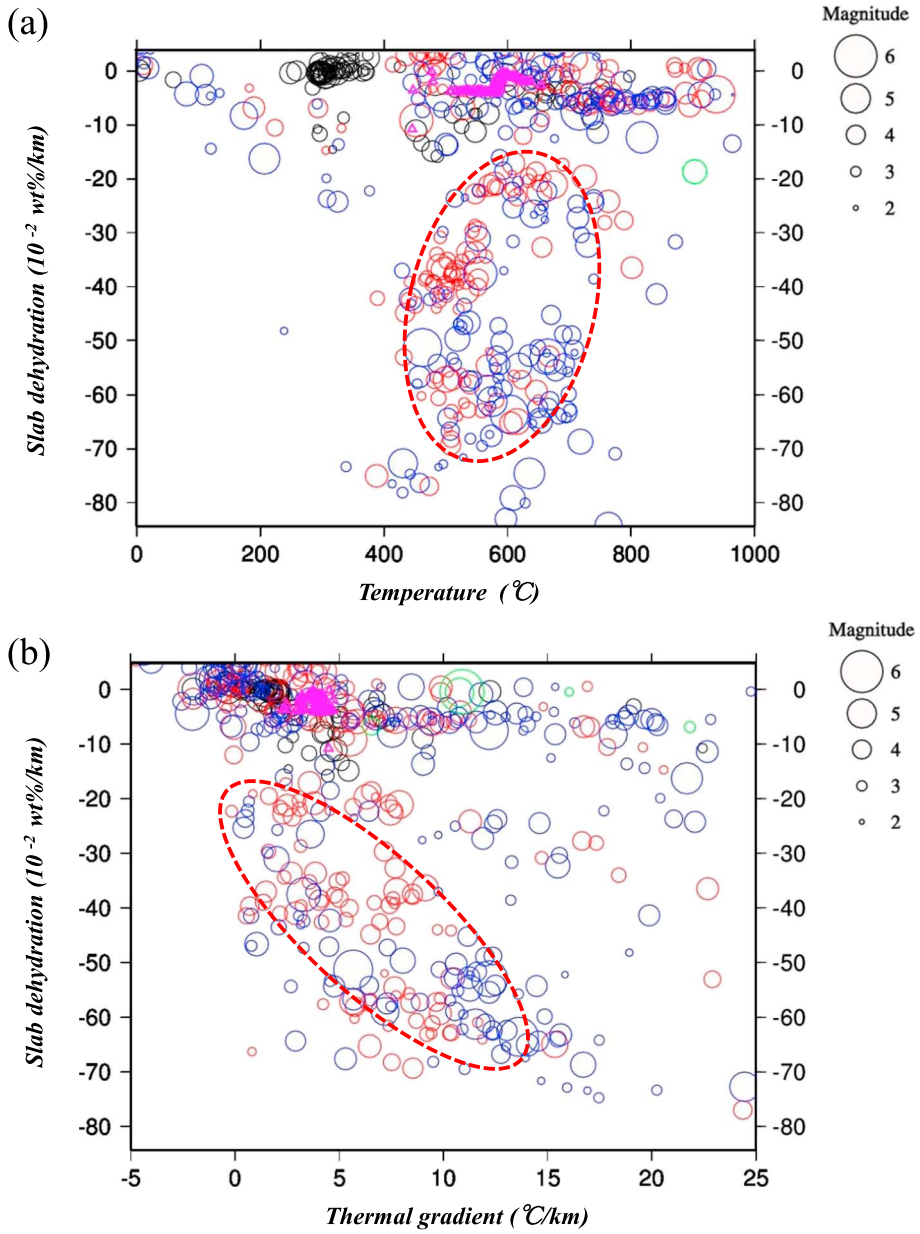

Figure 11. (a) The relationship between the slab dehydration and temperatures. The horizontal axis indicates the temperature at the hypocenters of >M2 earthquakes recorded by Geonet from 1 January 2001 to 31 December 2015. The vertical axis indicates the slab dehydration at the hypocenters. The open circles are hypocenters with the color showing the depth ranges. The pink open triangles indicate the possible slab dehydration condition for the tectonic tremors. The dashed red oval represents a swarm of intraslab earthquakes beneath the KMR region, where a high slab dehydration (wt%/km) and the corresponding temperature range (°C) are identifiable. (b) The relationship between the slab dehydration and the thermal gradient.

serpentinite into olivine and its effect on slab rheology, possibly leading to strengthening or embrittlement, as we can see that the intraslab earthquakes cluster more near the phase boundaries between serpentinite, chrolite, and harzburgite (Figure 9c). The intraslab earthquakes in northern Hikurangi (red circles) are distributed deeper on average than those in southern Hikurangi (blue circles) in the downdip direction. More investigations based on a higher-resolution model could be productive if finer analyses are available for the intraslab thermal and hydrous states.

The ordinary earthquakes and tectonic tremors in Hikurangi observed by Geonet with depths of −2 to 80 km below the plate interface are plotted in Figures 10 and 11. The intraslab earthquakes in zones of high slab

dehydration are primarily distributed in the KMR region. The maximum slab dehydration at the hypocenters of the earthquakes reached nearly 80×10^{-2} wt%/km in 2011 (circles at the bottom of Figure 10). The open blue circles represent earthquakes in the lower oceanic plate and reflect the existence of large amounts of dehydration in the ultramafic minerals in this region. The increase in the earthquake activity was concurrent with the tectonic tremors (open pink triangles) between 2008 and 2012 (Figure 10). The temporal fluctuation in the slab dehydration and subsequent regular earthquakes induced by slow earthquakes may explain this synchronization. Wallace et al. (2017) suggested that in addition to the shallow SSEs (<15 km) triggered off the east coast, they observed deeper SSEs (>30 km) in the Kapiti region as well as afterslip on the plate interface beneath the region of large coseismic slip on crustal faults in the 2016 Mw7.8 Kaikoura earthquake. Recent studies (e.g., Ikari et al., 2013; Okazaki & Hirth, 2016) have suggested that SSEs and the dehydration of lawsonite could directly trigger regular earthquakes in the subducting oceanic crust. The coexistence of slow earthquakes and adjacent regular earthquakes in Manawatu may be partly attributed to this effect, although the mechanism underlying this phenomenon remains poorly understood. Figure 11a shows that the slab dehydration at the hypocenters in the KMR region varies but is constrained by a temperature range of 400–800 °C and that the slab dehydration exceeds an absolute value of 0.2 wt%/km (dashed red oval). Similarly, a high slab thermal gradient associated with a high horizontal temperature gradient is also identified in the ultramafic rocks (open red and blue circles in the dashed red oval) of the Hikurangi Plateau in the KMR region (Figure 11b).

The high slab dehydration and a high-temperature gradient in the KMR region are conjectured to play important roles in the pore fluid pressure variations within microcracks or along the fractured interface and possibly to trigger both slow and regular earthquakes. This interpretation also applies to mechanical dehydration in the sediment layer, such as in the fore-arc offshore of the Hawke's Bay-Mahia Peninsula-Poverty Bay zone, where temperatures as low as 100 °C (Figure 6a) and the occurrence of SSEs have been identified (Figure 8).

5. Conclusions

Using a 3-D time-dependent thermal model, we investigated the thermal, water content and slab dehydration distributions in the subducted Hikurangi Plateau beneath the North Island, and our models indicate the following:

1. A large slab dehydration (>0.05 wt%/km) and a high thermal gradient (>4 °C/km) were identified beneath the seismically active band in the Kapiti-Manawatu-Raukumara region, where swarms of tectonic tremors and SSEs have also been observed.
2. The interplate slab dehydration is as high as 0.10 wt%/km beneath central Hikurangi and 0.12 wt%/km beneath southern Hikurangi, which contributes to the higher pore fluid pressure in southern Hikurangi. The dehydration-derived fluids could contribute to the along-arc variability of the interplate pore fluid pressure.
3. The tectonic tremors beneath Manawatu are associated with a high slab dehydration of >0.2 wt%/km and a temperature gradient of >10 °C/km. The interplate earthquakes recorded beneath Hikurangi are associated with phase transformations of hydrous MORB assemblages from lawsonite blueschist to greenschist, amphibolite, and eclogite. The mechanism by which dehydration-derived fluids trigger tectonic tremors and adjacent regular earthquakes beneath Hikurangi remains unclear.

Acknowledgments
We thank P. Tackley for sharing the source code Stag3D. We thank S. Ide for providing the tectonic tremor data at Hikurangi. We thank two anonymous reviewers for their constructive comments. We acknowledge the New Zealand GeoNet project and its sponsors EQC, GNS Science and LINZ, and Centennial database (USGS Earthquake Hazards Program) for providing data used in this study. All the figures are created by the Generic Mapping Tools (GMT) developed by Wessel and Smith (1998) and the Paraview software developed by Kitware Inc. This study is partly supported by JSPS KAKENHI grants 16H04040 and 16H06477. The data for this paper are available at DataOne dataset https://doi.org/10.15146/R30029.

References

Ansell, J. H., & Bannister, S. C. (1996). Shallow morphology of the subducted Pacific plate along the Hikurangi margin, New Zealand. *Physics of the Earth and Planetary Interiors*, *93*(1-2), 3–20. https://doi.org/10.1016/0031-9201(95)03085-9

Audet, P., Bostock, M. G., Christensen, N. I., & Peacock, S. M. (2009). Seismic evidence for overpressured subducted oceanic crust and megathrust fault sealing. *Nature*, *457*(7225), 76–78. https://doi.org/10.1038/nature07650

Bai, Y., Lay, T., Cheung, K. F., & Ye, L. (2017). Two regions of seafloor deformation generated the tsunami for the 13 November 2016, Kaikoura, New Zealand earthquake. *Geophysical Research Letters*, *44*, 6597–6606. https://doi.org/10.1002/2017GL073717

Bassett, D., Sutherland, R., & Henrys, S. (2014). Slow wave speeds and fluid overpressure in a region of shallow geodetic locking and slow slip, Hikurangi subduction margin, New Zealand. *Earth and Planetary Science Letters*, *389*, 1–13. https://doi.org/10.1016/j.epsl.2013.12.021

Bell, R., Sutherland, R., Barker, D. H. N., Henrys, S., Bannister, S., Wallace, L., & Beavan, J. (2010). Seismic reflection character of the Hikurangi subduction interface, New Zealand, in the region of repeated Gisborne slow slip events. *Geophysical Journal International*, *180*(1), 34–48. https://doi.org/10.1111/j.1365-246X.2009.04401.x

Beroza, G. C., & Ide, S. (2011). Slow earthquakes and nonvolcanic tremors. *Annual Review of Earth and Planetary Sciences*, *39*(1), 271–296. https://doi.org/10.1146/annurev-earth-040809-152531

Billen, M. I., & Hirth, G. (2007). Rheologic controls on slab dynamics. *Geochemistry, Geophysics, Geosystems*, *8*, Q08012. https://doi.org/10.1029/2007GC001597

Burkett, E. R., & Billen, M. I. (2010). Three-dimensionality of slab detachment due to ridge-trench collision: Laterally simultaneous boudinage versus tear propagation. *Geochemistry, Geophysics, Geosystems*, *11*, Q11012. https://doi.org/10.1029/2010GC003286

Byerlee, J. D. (1978). Friction of rocks. *Pure and Applied Geophysics*, *116*(4-5), 615–626. https://doi.org/10.1007/BF00876528

Clift, P., & Vannucchi, P. (2004). Controls on tectonic accretion versus erosion in subduction zones: Implications for the origin and recycling of the continental crust. *Reviews of Geophysics*, *42*, RG2001. https://doi.org/10.1029/2003RG000127

Cochran, U. A., Berryman, K. R., Zachariasen, J., Mildenhall, D. C., Hayward, B. W., Southall, K., et al. (2006). Paleoecological insights into subduction zone earthquake occurrence, eastern North Island, New Zealand. *Geological Society of America Bulletin*, *118*(9-10), 1051–1074. https://doi.org/10.1130/B25761.1

DeMets, C., Gordon, R. G., & Argus, D. F. (2010). Geologically current plate motions. *Geophysical Journal International*, *181*(1), 1–80. https://doi.org/10.1111/j.1365-246X.2009.04491.x

Dragert, H., Wang, K., & James, T. S. (2001). A silent slip event on the deeper Cascadia subduction interface. *Science*, *292*(5521), 1525–1528. https://doi.org/10.1126/science.1060152

Ellis, S., Fagereng, A., Barker, D., Henrys, S., Saffer, D., Wallace, L., et al. (2015). Fluid budgets along the northern Hikurangi subduction margin, New Zealand: The effect of a subducting seamount on fluid pressure. *Geophysical Journal International*, *202*(1), 277–297. https://doi.org/10.1093/gji/ggv127

Engdahl, E. R., & Villasenor, A. (2002). Global seismicity: 1900–1999. In W. H. K. Lee, et al. (Eds.), *International Handbook of Earthquake and Engineering Seismology, Part A* (chap. 41, pp. 665–690). Cambridge, MA: Academic Press. https://doi.org/10.1016/S0074-6142(02)80244-3

Fagereng, A., & Ellis, S. (2009). On factors controlling the depth of interseismic coupling on the Hikurangi subduction interface, New Zealand. *Earth and Planetary Science Letters*, *278*(1-2), 120–130. https://doi.org/10.1016/j.epsl.2008.11.033

Furlong, K. P., & Herman, M. (2017). Reconciling the deformational dichotomy of the 2016 *Mw* 7.8 Kaikoura New Zealand earthquake. *Geophysical Research Letters*, *44*, 6788–6791. https://doi.org/10.1002/2017GL074365

Gao, X., & Wang, K. (2014). Strength of stick-slip and creeping subduction megathrusts from heat flow observations. *Science*, *345*(6200), 1038–1041. https://doi.org/10.1126/science.1255487

Grose, C. J., & Afonso, J. C. (2013). Comprehensive plate models for the thermal evolution of oceanic lithosphere. *Geochemistry, Geophysics, Geosystems*, *14*, 3751–3778. https://doi.org/10.1002/ggge.20232

Hacker, B. R., Abers, G. A., & Peacock, S. M. (2003). Subduction factory 1. Simplified mineralogy, densities, seismic wave speeds, and H_2O contents. *Journal of Geophysical Research*, *108*(B1), 2029. https://doi.org/10.1029/2001JB001127

Hacker, B. R., Peacock, S. M., Abers, G. A., & Holloway, S. D. (2003). Subduction factory 2. Are intermediate-depth earthquakes in subducting slabs linked to metamorphic dehydration reactions? *Journal of Geophysical Research*, *108*(B1), 2030. https://doi.org/10.1029/2001JB001129

Hall, C. E., & Parmentier, E. M. (2003). Influence of grain size evolution on convective instability. *Geochemistry, Geophysics, Geosystems*, *4*(3), 1029. https://doi.org/10.1029/2002GC000308

Hardebeck, J. L., & Loveless, J. P. (2017). Creeping subduction zones are weaker than locked subduction zones. *Nature Geoscience*, *11*(1), 60–64. https://doi.org/10.1038/s41561-017-0032-1

Hayward, B. W., Grenfell, H. R., Sabaa, A. T., Carter, R., Cochran, U., Lipps, J. H., et al. (2006). Micropaleontological evidence of large earthquakes in the past 7200 years in southern Hawke's Bay, New Zealand. *Quaternary Science Reviews*, *25*(11-12), 1186–1207. https://doi.org/10.1016/j.quascirev.2005.10.013

Henrys, S. A., Ellis, S., & Uruski, C. (2003). Conductive heat flow variations from bottom-simulating reflectors on the Hikurangi margin, New Zealand. *Geophysical Research Letters*, *30*(2), 1065. https://doi.org/10.1029/2002GL015772

Hirth, G., & Kohlstedt, D. (2003). In J. Eiler (Ed.), *Rheology of the upper mantle and the mantle wedge: A view from the experimentalists, inside the subduction factory*, *Geophysical Monograph Series* (Vol. 138, pp. 83–105). Washington, DC: American Geophysical Union.

Hyndman, R. D., & Wang, K. (1993). The rupture zone of Cascadia great earthquakes from current deformation and the thermal regime. *Journal of Geophysical Research*, *98*(B2), 2039–2060. https://doi.org/10.1029/92JB02279

Hyndman, R. D., Wang, K., & Yamano, M. (1995). Thermal constraints on the seismogenic portion of the southwestern Japan subduction thrust. *Journal of Geophysical Research*, *100*(B8), 15,373–15,392. https://doi.org/10.1029/95JB00153

Idehara, K., Yabe, S., & Ide, S. (2014). Regional and global variations in the temporal clustering of tectonic tremor activity. *Earth, Planets and Space*, *66*, 66. https://doi.org/10.1186/1880-5981-66-66

Ikari, M. J., Marone, C., Saffer, D. M., & Kopf, A. J. (2013). Slip weakening as a mechanism for slow earthquakes. *Nature Geoscience*, *6*(6), 468–472. https://doi.org/10.1038/ngeo1818

Jadamec, M. A., & Billen, M. I. (2010). Reconciling surface plate motions with rapid threedimensional mantle flow around a slab edge. *Nature*, *465*(7296), 338–341. https://doi.org/10.1038/nature09053

Ji, Y., & Yoshioka, S. (2017). Slab dehydration and earthquake distribution beneath southwestern and Central Japan based on three-dimensional thermal modeling. *Geophysical Research Letters*, *44*, 2679–2686. https://doi.org/10.1002/2016GL072295

Ji, Y., Yoshioka, S., & Banay, Y. A. (2017). Thermal state, slab metamorphism and interface seismicity in the Cascadia subduction zone based on 3-D modeling: 3-D thermomechanical model for Cascadia. *Geophysical Research Letters*, *44*, 9242–9252. https://doi.org/10.1002/2017GL074826

Ji, Y., Yoshioka, S., & Matsumoto, T. (2016). Three-dimensional numerical modeling of temperature and mantle flow fields associated with subduction of the Philippine Sea plate, southwest Japan. *Journal of Geophysical Research*, *121*, 4458–4482. https://doi.org/10.1002/2016JB012912

Lewis, K. B., Collot, J. Y., & Lallemande, S. E. (1998). The dammed Hikurangi Trough: A channel-fed trench blocked by subducting seamounts and their wake avalanches (New Zealand–France GeodyNZ Project). *Basin Research*, *10*(4), 441–468. https://doi.org/10.1046/j.1365-2117.1998.00080.x

Liu, Z., Owen, S., Dong, D., Lundgren, P., Webb, F., Hetland, E., & Simons, M. (2010). Estimation of interplate coupling in the Nankai trough, Japan using GPS data from 1996 to 2006. *Geophysical Journal International*, *181*, 1313–1328. https://doi.org/10.1111/j.1365-246X.2010.04600.x

McCaffrey, R., Wallace, L. M., & Beavan, J. (2008). Slow slip and frictional transition at low temperature at the Hikurangi subduction zone. *Nature Geoscience*, *1*(5), 316–320. https://doi.org/10.1038/ngeo178

McKenzie, D. P. (1967). Some remarks on heat flow and gravity anomalies. *Journal of Geophysical Research*, *72*(24), 6261–6273.

Montserrat, S., Tamburrino, A., Roche, O., & Niño, Y. (2012). Pore fluid pressure diffusion in defluidizing granular columns. *Journal of Geophysical Research*, *117*, F02034. https://doi.org/10.1029/2011JF002164

Müller, R. D., Sdrolias, M., Gaina, C., & Roest, W. R. (2008). Age, spreading rates, and spreading asymmetry of the world's ocean crust. *Geochemistry, Geophysics, Geosystems*, *9*, Q04006. https://doi.org/10.1029/2007GC001743

Obara, K. (2002). Nonvolcanic deep tremor associated with subduction in southwest Japan. *Science*, *296*(5573), 1679–1681. https://doi.org/10.1126/science.1070378

Okazaki, K., & Hirth, G. (2016). Dehydration of lawsonite could directly trigger earthquakes in subducting oceanic crust. *Nature*, *530*, 81–84.

Omori, S., Kita, S., Maruyama, S., & Santosh, M. (2009). Pressure-temperature conditions of ongoing regional metamorphism beneath the Japanese Islands. *Gondwana Research*, *16*(3-4), 458–469. https://doi.org/10.1016/j.gr.2009.07.003

Pollack, H. N., Hurter, S. J., & Johnson, J. R. (1993). Heat flow from the Earth's interior: Analysis of the global data set. *Reviews of Geophysics*, *31*(3), 267–280. https://doi.org/10.1029/93RG01249

Ranalli, G. (1995). *Rheology of the Earth* (413 pp.). Berlin, Germany: Springer Science and Business Media.

Rogers, G., & Dragert, H. (2003). Episodic tremor and slip on the Cascadia subduction zone: The chatter of silent slip. *Science*, *300*(5627), 1942–1943. https://doi.org/10.1126/science.1084783

Saffer, D. M., & Wallace, L. M. (2015). The frictional, hydrologic, metamorphic and thermal habitat of shallow slow earthquakes. *Nature Geoscience*, *8*(8), 594–600. https://doi.org/10.1038/ngeo2490

Stein, C. A., & Stein, S. (1992). A model for the global variation in oceanic depth and heat flow with lithospheric age. *Nature*, *359*(6391), 123.

Stirling, M. W., McVerry, G. H., & Berryman, K. R. (2002). A new seismic hazard model of New Zealand. *Bulletin of the Seismological Society of America*, *92*(5), 1878–1903. https://doi.org/10.1785/0120010156

Stirling, M. W., McVerry, G. H., Gerstenberger, M., Litchfield, N., Van Dissen, R., Berryman, K., et al. (2012). National Seismic Hazard Model for New Zealand: 2010 update. *Bulletin of the Seismological Society of America*, *102*(4), 1514–1542. https://doi.org/10.1785/0120110170

Tackley, P. J., & Xie, S. (2003). Stag3d: A code for modeling thermo-chemical multiphase convection in Earth's mantle. In K. J. Bathe (Ed.), *Computational Fluid and Solid Mechanics 2003* (pp. 1524–1527). Amsterdam, Netherlands: Elsevier B.V.

Townend, J. (1997). Estimates of conductive heat flow through bottom-simulating reflectors on the Hikurangi and southwest Fiordland continental margins, New Zealand. *Marine Geology*, *141*(1–4), 209–220. https://doi.org/10.1016/s0025-3227(97)00073-x

van Keken, P. E., Hacker, B. R., Syracuse, E. M., & Abers, G. A. (2011). Subduction factory: 4. Depth-dependent flux of H_2O from subducting slabs worldwide. *Journal of Geophysical Research*, *116*, B01401. https://doi.org/10.1029/2010JB007922

Wada, I., Behn, M. D., & Shaw, A. M. (2012). Effects of heterogeneous hydration in the incoming plate, slab rehydration, and mantle wedge hydration on slab-derived H2O flux in subduction zones. *Earth and Planetary Science Letters*, *353*, 60–71.

Wada, I., & Wang, K. (2009). Common depth of slab-mantle decoupling: Reconciling diversity and uniformity of subduction zones. *Geochemistry, Geophysics, Geosystems*, *10*, Q10009. https://doi.org/10.1029/2009GC002570

Wallace, L. M., Beavan, J., McCaffrey, R., & Darby, D. (2004). Subduction zone coupling and tectonic block rotations in the North Island, New Zealand. *Journal of Geophysical Research*, *109*, B12406. https://doi.org/10.1029/2004JB003241

Wallace, L. M., & Eberhart-Phillips, D. (2013). Newly observed, deep slow slip events at the central Hikurangi margin, New Zealand: Implications for downdip variability of slow slip and tremor, and relationship to seismic structure. *Geophysical Research Letters*, *40*, 5393–5398. https://doi.org/10.1002/2013GL057682

Wallace, L. M., Kaneko, K., D'Anastasio, E., Hreinsdottir, S., Bartlow, N., Fry, B., et al. (2017). Widespread slow slip events triggered at the Hikurangi subduction zone by the M7.8 Kaikoura earthquake, New Zealand, *JPGU-AGU Joint Meeting*, *2017*, SSS04–SSS23.

Wallace, L. M., Reyners, M., Cochran, U., Bannister, S., Berryman, K., Downes, G., et al. (2009). Characterizing the seismogenic zone of a major plate boundary subduction thrust: Hikurangi Margin, New Zealand. *Geochemistry, Geophysics, Geosystems*, *10*, Q10006. https://doi.org/10.1029/2009GC002610

Wallace, L. M., Webb, S. C., Ito, Y., Mochizuki, K., Hino, R., Henrys, S., et al. (2016). Slow slip near the trench at the Hikurangi subduction zone, New Zealand. *Science*, *352*(6286), 701–704. https://doi.org/10.1126/science.aaf2349

Wang, K., Hyndman, R. D., & Yamano, M. (1995). Thermal regime of the southwest Japan subduction zone: Effects of age history of the subducting plate. *Tectonophysics*, *248*(1-2), 53–69. https://doi.org/10.1016/0040-1951(95)00028-L

Wech, A. G. (2016). Extending Alaska's plate boundary: Tectonic tremor generated by Yakutat subduction. *Geology*, *44*(7), 587–590. https://doi.org/10.1130/G37817.1

Wech, A. G., & Creager, K. C. (2011). A continuum of stress, strength and slip in the Cascadia subduction zone. *Nature Geoscience*, *4*(9), 624–628. https://doi.org/10.1038/ngeo1215

Wessel, P., & Smith, W. H. F. (1998). New, improved version of the generic mapping tools released. *Eos Transactions American Geophysical Union*, *79*(47), 579. https://doi.org/10.1029/98EO00426

Williams, C. A., Eberhart-Phillips, D., Bannister, S., Barker, D. H. N., Henrys, S., Reyners, M., & Sutherland, R. (2013). Revised interface geometry for the Hikurangi subduction zone. *New Zealand*. *Seismological Research Letters*, *84*(6), 1066–1073. https://doi.org/10.1785/0220130035

Yabe, S., Ide, S., & Yoshioka, S. (2014). Along-strike variations in temperature and tectonic tremor activity along the Hikurangi subduction zone, New Zealand. *Earth, Planets and Space*, *66*(1), 142. https://doi.org/10.1186/s40623-014-0142-6

Yoshii, T. (1975). Regionality of group velocities of Rayleigh waves in the Pacific and thickening of the plate. *Earth and Planetary Science Letters*, *25*(3), 305–312. https://doi.org/10.1016/0012-821X(75)90246-0

Yoshioka, S., Mikumo, T., Kostoglodov, V., Larson, K. M., Lowry, A. R., & Singh, S. K. (2004). Interplate coupling and a recent aseismic slow slip event in the Guerrero seismic gap of the Mexican subduction zone, as deduced from GPS data inversion using a Bayesian information criterion. *Physics of the Earth and Planetary Interiors*, *146*(3–4), 513–530. https://doi.org/10.1016/j.pepi.2004.05.006

Yoshioka, S., & Murakami, K. (2007). Temperature distribution of the upper surface of the subducted Philippine Sea plate, southwest Japan, from a three-dimensional subduction model: Relation to large interplate and low-frequency earthquakes. *Geophysical Journal International*, *171*(1), 302–315. https://doi.org/10.1111/j.1365-246X.2007.03510.x